ACS Sustainable Chemistry & Engineering

Research Article

pubs.acs.org/journal/ascecg

Self-Assembly of Semiconductor Nanoparticles/Reduced Graphene Oxide (RGO) Composite Aerogels for Enhanced Photocatalytic Performance and Facile Recycling in Aqueous Photocatalysis

Wenjun Liu, Jingyu Cai, and Zhaohui Li*

Research Institute of Photocatalysis, State Key Laboratory of Photocatalysis on Energy and Environment, College of Chemistry, Fuzhou University, #523 Gongye Road, Fuzhou 350002, People's Republic of China

Supporting Information

ABSTRACT: A BiOBr/reduced graphene oxide (RGO) composite aerogel with BiOBr nanoplates grown on an interconnected three-dimensional RGO-based porous network was prepared by one-pot hydrothermal method using L-lysine as a reducing agent and the cross-linker. Its enhanced adsorption toward pollutants owing to its large Brunauer–Emmett–Teller specific surface area and spongy nature, improved light absorption due to its extremely lightweight nature and the RGO promoting photogenerated charge separation contributed to the BiOBr/RGO aerogel's enhanced activity for photocatalytic degradation in an aqueous system. The BiOBr/RGO aerogel also showed high stability and can be easily separated from the reaction systems for recycling. The facile one-pot method has been proved to be generic in the formations of different semiconductor embedded RGO aerogels like BiOX/RGO (X = Cl and I), CdS/RGO and Fe_2O_3/RGO aerogels, which combine the advantages of enhanced photocatalytic activity with facile recycling for applications in aqueous photocatalytic reaction systems.

KEYWORDS: *RGO aerogel, BiOBr, Photocatalysis, Organic pollutants, Recycle*

INTRODUCTION

Aerogels are three-dimensional (3D) networks consisting of interpenetrating micropores and mesopores.[1] Among the already investigated aerogels, reduced graphene oxide (RGO)-based aerogels have attracted extensive attention due to their peculiar properties, including low density, high surface area, large open pores, as well as those translated from the RGO building block.[2,3] Fabricated from GO as the starting building block and a variety of cross-linkers, RGO-based aerogels with good mechanical and thermal strength have already shown potentials in a variety of applications, such as solar cells,[4] lithium-ion batteries,[5−7] various sensors,[8] water purifications[9−11] and in other systems.[12,13]

In the past decades, semiconductor-based photocatalysis has been widely employed in the treatment of organic contaminants in aqueous systems.[14,15] For practical applications in aqueous systems, it is ideal to immobilize the nanostructured photocatalysts on certain solid surfaces for easy separation and recycling. For this purpose, a variety of solid materials have already been investigated for use as supports in photocatalysis.[16] Usually, an ideal support should have a large specific surface area, open pores for fast mass transportation and surface sites for anchoring of the catalysts. RGO aerogel fulfills all the requirements for a good support and, especially, its lightweight makes it capable of floating on the surface of an aqueous reaction system, which allows it to absorb more solar irradiations. More than these, the RGO building block can promote the separation of photogenerated electrons and holes, which would greatly enhance the performance of photocatalysts.[17] All these peculiar properties of RGO aerogel make it especially appealing as a support for semiconductor photocatalysts. However, although RGO incorporated semiconductor photocatalysts have been well studied,[18−23] the investigations on the formation of semiconductor/RGO composite aerogels with focus on their applications in photocatalysis is limited.[24−27]

In this paper, for the first time we demonstrated a facile one-pot hydrothermal method to fabricate BiOBr/RGO composite aerogel using lysine as a reducing agent and cross-linker. BiOBr has attracted extensive recent attentions as a promising photocatalyst due to its capability of response to visible-light, its chemical stability and superior activity.[28−31] Although BiOBr is promising in photocatalysis, its low specific surface area and the inherent difficulty for the nanostructured powders to be separated from the reaction systems hinder its practical applications. By embedding BiOBr in RGO aerogel, the as-formed BiOBr/RGO composite aerogel shows excellent performance in the photocatalytic degradation of a dye under visible light. The photocatalyst can float on water, showing impressive performance in terms of its activity and stability. After reaction, it is capable of removing it with a tweezers and reusing it with unvaried performance. The facile one-pot

Received: October 10, 2014
Revised: December 16, 2014
Published: January 12, 2015

DOI: 10.1021/sc5006473
ACS Sustainable Chem. Eng. 2015, 3, 277−282

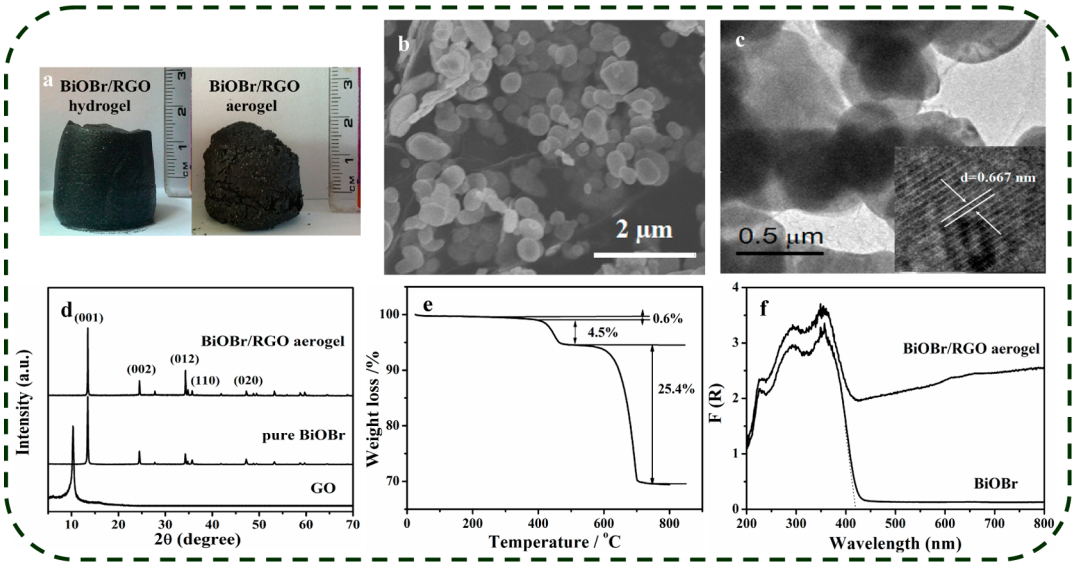

Figure 1. (a) Photographs of BiOBr/RGO hydrogel and the corresponding aerogel; (b) SEM image of BiOBr/RGO aerogel; (c) TEM image of BiOBr/RGO aerogel (inset HRTEM image); (d) XRD patterns for BiOBr/RGO aerogel, BiOBr and GO; (e) TGA of BiOBr/RGO aerogel in air from 30 to 800 °C (at a rate of 5 °C/min); (f) UV/vis DRS spectra of BiOBr/RGO aerogel and pure BiOBr.

method can also be applied to the formations of other semiconductor photocatalysts embedded RGO composite aerogels, like BiOX/RGO (X = Cl and I), CdS/RGO and Fe_2O_3/RGO aerogels.

EXPERIMENTAL SECTION

Graphite flake (99.8%, 325 mesh) and $BiBr_3$ (99%) were provided by Alfa. $BiCl_3$ (AR), BiI_3 (AR), $NaNO_3$ (AR), $Cd(NO_3)_2$ (AR), $Fe(NO_3)_3$ (AR) and L-lysine (AR) were provided by Aladdin. All the reagents were used without further purification.

Graphene oxide (GO) was synthesized from graphite flake using a modified Hummers methods.[32] For the preparation of BiOBr/RGO hydrogels, GO aqueous dispersion (20 mL, 5 mg/mL) was added into a 50 mL solution containing $BiBr_3$ and L-lysine (L-lys) under vigorous magnetic stirring. After 30 min, the solution was transferred to a Teflon-sealed autoclave and heated at 160 °C for 10 h to obtain the cylinder hydrogels. The as-obtained hydrogels were washed with deionized water to remove remnant ions. After that, the hydrogels were freeze-dried to obtain the aerogels. The BiOCl/RGO, BiOI/RGO, CdS/RGO and Fe_2O_3/RGO aerogels were prepared from $BiCl_3$, BiI_3, $Cd(NO_3)_2$ and $Fe(NO_3)_3$ with GO respectively under otherwise similar conditions. Pure BiOBr powder was prepared similarly from $BiBr_3$ in the absence of GO.

The morphology of the samples was characterized by a field emission scanning electron microscopy (SEM, JSM-6700F). The transmission electron microscopy (TEM) and high-resolution transmission electron microscopy (HRTEM) images were measured by a JEOL model JEM 2010 EX instrument at an accelerating voltage of 200 kV. Powder X-ray diffraction (XRD) data were collected using a Bruker D8 Advance X-ray diffractometer (Cu Kα_1 irradiation, λ = 1.5406 Å). Thermogravimetric analysis (TGA) of the sample was performed on a Pyris Diamond TG/DTA thermogravimetric analyzer (PerkinElmer Thermal Analysis). Samples were heated under an air atmosphere from 30 to 800 °C at 5 °C/min. Raman spectroscopic study was performed using an inVia-Reflex Micro-Raman Spectroscopy system (Renishaw Co.) with 532 nm line of an Ar ion laser at room temperature. Fourier transform infrared (FT-IR) spectra were recorded in transmittance mode with a resolution of 4 cm^{-1} using a Nicolet Nexus 670 FTIR spectrometer and 5 mg of catalyst. X-ray photoelectron spectroscopy (XPS) measurements were performed on a PHI Quantum 2000 XPS system with a monochromatic Al Kα source and a charge neutralizer. All the binding energies were referred to the C 1s peak at 284.6 eV of the surface adventitious carbon. The total organic carbon concentration (TOC) was conducted in Shimadzu TOC-V (CPH) total carbon analyzer. The electrical conductivity of the composites was determined by measuring the volume resistivity (Ω·cm) by the four-probe method.

The photocatalytic activity of sample was evaluated in terms of the degradation of rhodamine B (RhB, 20 mg/L). The BiOBr/RGO was added into a 100 mL quartz photoreactor containing 60 mL of RhB solution. A 300 W Xe lamp with a 420 nm cutoff filter was used as a visible light source, providing illumination intensity of 0.35 W/cm^2 at the sample surface. At the given time intervals, the analytical samples were taken from the mixture and analyzed by recording variations in the absorption in UV−vis spectra of RhB using a Cary 500 ultraviolet visible spectrometer.

RESULTS AND DISCUSSION

The BiOBr/RGO hydrogels were prepared from GO and $BiBr_3$ hydrothermally using L-lysine as both cross-linker and reducing agent. Our previous studies on the formation of RGO aerogels using lysine revealed that the optimum condition to obtain the RGO hydrogel is at a weight ratio of GO to L-lysine ($r_{G/L}$) of 1:2.[10] Therefore, the weight ratio of GO to L-lysine ($r_{G/L}$) was set at 1:2, while the examined weight ratio of GO to $BiBr_3$ ($r_{G/B}$) ranged from 1:2.5 to 1:10. It was found that well shaped hydrogels can be obtained in the whole examined ranges. The hydrogels obtained have a 3D cylindrical morphology in the macroscopic views, which conform to that of the vessel. The size of the obtained hydrogels only varied a little with the ratio of $r_{G/B}$ (Figure S1, Supporting Information) and for $r_{G/B}$ at 1:10, the obtained cylinder has a diameter of approximately 25 mm and a height of 25 mm (Figure 1a). Upon freeze-dried, the as-prepared hydrogel was dehydrated with almost no shrinkage to obtain a three-dimensional monolithic aerogel. The SEM image of the as-obtained aerogel exhibits that the sample is comprised of RGO nanosheets interconnected to form a three-dimensional porous network with micrometer interconnected pores. Nanoplates with thickness of about 10 nm and the dimension ranged from 0.5 to 0.7 μm are densely anchored on the RGO nanosheets (Figure 1b). The existence of well dispersed nanoplates on the RGO nanosheets is also evidenced from the TEM image (Figure 1c). The high-resolution TEM

DOI: 10.1021/sc5006473
ACS Sustainable Chem. Eng. 2015, 3, 277−282

(HRTEM) image shows clear lattice fringe of 0.667 nm, corresponding to (001) crystallographic planes reflections of tetragonal BiOBr and indicated the formation of BiOBr (inset of Figure 1c).

The XRD pattern of the sample shows peaks of 2θ values at 13.3°, 24.3°, 34.3°, 35.7° and 47.3°, which correspond to the (001), (002), (012), (110) and (020) crystallographic planes of tetragonal BiOBr (JCPDF 01-073-2061) (Figure 1d). Although no diffractions peaks corresponding to either GO or RGO has been observed in the XRD pattern of the resultant product, the FT-IR spectra of the product shows peaks at 1730, 1573, 1382 and 1205 cm^{-1}, corresponding to C═O, −C═C−, −OH and C—O and confirmation of the successful incorporation of the carbon additive. As compared to pristine GO, the much weaker peaks of C═O and −OH on the product demonstrates that GO has been successfully reduced during the aerogel formation process (Figure S2a, Supporting Information). Accordingly, the Raman spectrum of shows that the intensity ratio of the D band and G band (I_D/I_G = 1.01) is higher as compared with that of GO (I_D/I_G = 0.95), indicating the introduction of defects during the formation of the BiOBr/RGO aerogel (Figure S2b, Supporting Information).[33] The reduction of GO has also been evidenced from the XPS spectra of the BiOBr/RGO aerogel. The XPS spectrum in the C 1s region reveals that the oxygen-bound carbon content decreases from the original 55.0% in GO to 21.3%, indicating a high degree of GO was reduced during the hydrothermal gelation process (Figure S2c, Supporting Information).[34] To quantify the amount of RGO in the BiOBr/RGO aerogel, thermogravimetric analysis (TGA) was carried out from 30 to 800 °C. As shown in Figure 1e, the weight loss (4.5%) in the temperature range of 395−490 °C corresponds to the amount of RGO characterizations confirmed that the BiOBr/RGO aerogel has been successfully obtained.

The formation of the BiOBr/RGO aerogel using L-lysine is depicted in Scheme 1. It is generally known that $BiBr_3$ would

Scheme 1. Schematic Illustration of the Formation of BiOBr/RGO Hydrogel and the Corresponding Aerogel

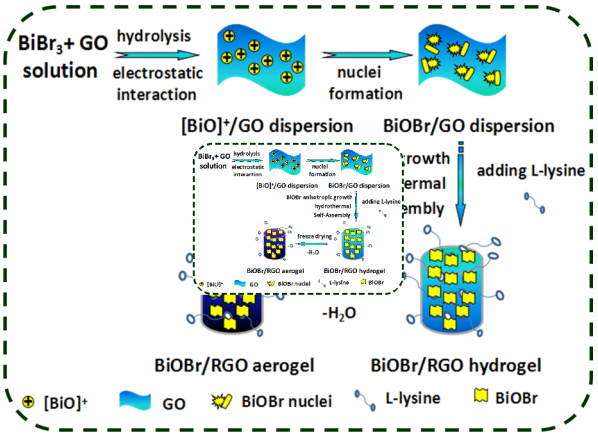

hydrolyze to form $[BiO]^+$ ions that can easily adsorb on the negative surface of GO owing to the electrostatic interaction.[35,36] BiOBr nuclei are spontaneously formed through the reaction between $[BiO]^+$ ions and Br^- ions on the GO surface. During the hydrothermal treatment, the an-isotropic growth of BiOBr nuclei lead to the formation of lamellar BiOBr on the GO surface, while in the meantime, GO is reduced to RGO. The existence of the electrostatic attraction and hydrogen bonds between the amino group of lysine and the carboxyl group on GO surface as well as the $\pi-\pi$ stacking between the GO help to form a 3D BiOBr/RGO composite hydrogel. Upon freeze-dried, the hydrogel is dehydrated to form the three-dimensional aerogel.

Due to the incorporation of the RGO, the BiOBr/RGO aerogel shows a relatively larger Brunauer−Emmett−Teller (BET) specific surface area of 15.77 m^2/g compared with that of the BiOBr powder (3.69 m^2/g) (Figure S3, Supporting Information). This value is even a little larger than that of pure RGO aerogel prepared similarly (11.8 m^2/g).[37] It is postulated that BiOBr nanoplates in RGO aerogles can act as a spacer to prevent aggregation of the RGO nanosheets. The less aggregation of RGO nanosheets on the composite aerogels as compared with that of pure RGO aerogel can also be evidenced from the SEM images (Figure 1b).[10] The introduction of RGO into the composite also results in the enhanced absorption in the visible light region, as shown in the UV/vis DRS spectrum of the BiOBr/RGO aerogel, in accordance with the color changed from the original yellow for pure BiOBr to dark gray for the BiOBr/RGO aerogel (Figure 1f). In addition to these, the BiOBr/RGO aerogel shows a low density of 0.05 g/cm^3 due to the existence of large open pores, as evidenced from the SEM image. Although this value is little higher than that of the pure RGO aerogel reported previously (0.003 g/cm^3), the aerogel can still float on the surface of the aqueous reaction system to ensure it for enhanced light absorption.[10] This makes the BiOBr/RGO aerogel extremely attractive for use as a photocatalyst for the degradation of organic pollutants in aqueous systems because it can float on the surface to absorb more visible-light energy, as compared to those powder photocatalysts that sink to the bottom. To demonstrate this, the photocatalytic degradation of RhB over the BiOBr/RGO aerogel under visible light irradiation was investigated and was compared with that of RGO aerogel and BiOBr powder. The temporal evolution of the spectral changes and the RhB concentration change was monitored by the maximum absorption of RhB at 554 nm during the photodegradation of RhB over the as-prepared BiOBr/RGO aerogel. As shown in Figure 2a, the decrease of the intensity of the main peak of RhB at 554 nm was accompanied by a concurrent gradual hypsochromic shift of the main peak to a shorter wavelength during the visible light irradiation. This gradual hypsochromic shift has been well established to be a step-by-step de-ethylation of RhB, whereas the decrease of the intensity indicates the cleavage of the whole conjugated chromophore structure of RhB.[38] This observation indicates that the photocatalytic degradation of RhB over the irradiated BiOBr/RGO aerogel proceeds via a simultaneous de-ethylation and the chromophore cleavage pathways. Decolorization of RhB solution can be achieved in 3 h over irradiated BiOBr/RGO aerogel and after irradiated for 5 h, all the peaks corresponding to RhB or its derivatives disappeared, indicating that RhB decomposed to small organics or CO_2. The TOC changed from the original 301.22 to 3.75 mg/L after 5 h of irradiation, further confirming that almost all RhB has been mineralized. On the contrary, no hypsochromic shift of the main peak of RhB at 554 nm was observed over the pure RGO aerogel during this period, which indicated that RhB was only adsorbed on the pure RGO aerogel (Figure S4, Supporting Information). In the meantime, a much lower efficiency was observed over the BiOBr powder. Only 35% of RhB had been converted after 5 h of visible light irradiation (Figure 2b). Besides this, the solution still

DOI: 10.1021/sc5006473
ACS Sustainable Chem. Eng. 2015, 3, 277−282

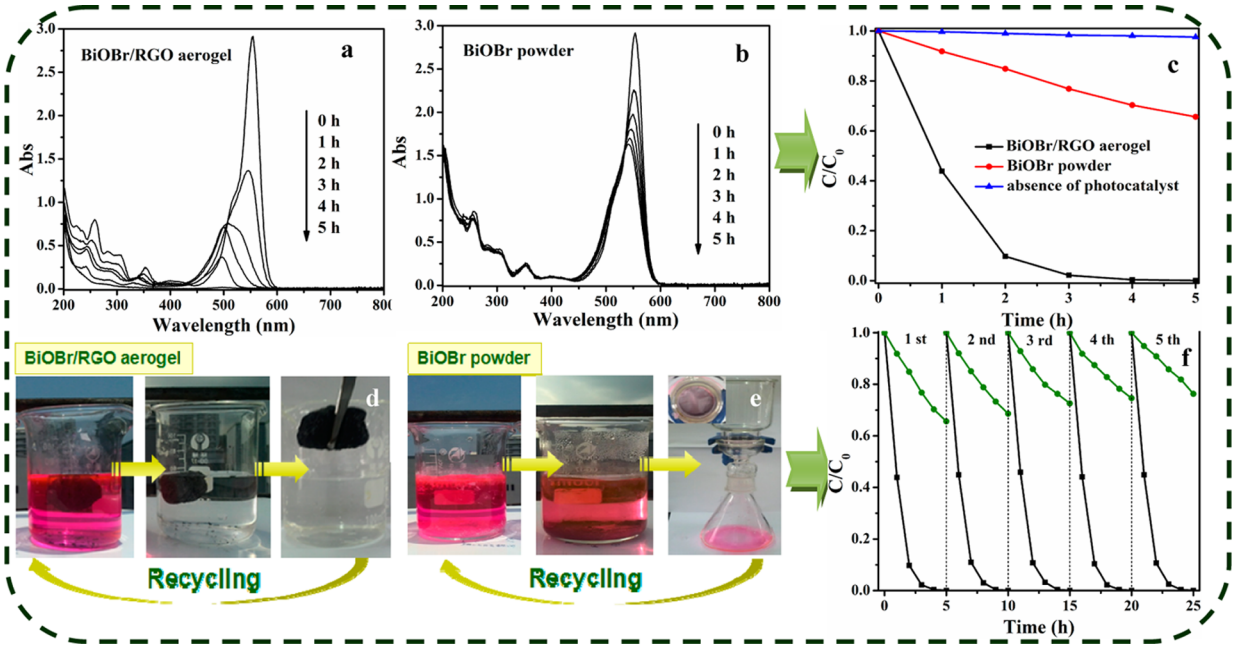

Figure 2. Temporal absorption spectral patterns of RhB during the photodegradation process over (a) BiOBr/RGO aerogel and (b) BiOBr powder; (c) comparison of the temporal changes of RhB concentration, as monitored by the UV−vis absorption spectra at 554 nm over irradiated BiOBr/RGO aerogel and BiOBr powder; photographs of the photodegradation and recycling processes under visible light irradiation over the as-prepared (d) BiOBr/RGO aerogel and (e) BiOBr powder; (f) cycling runs under visible light irradiation (black lines for BiOBr/RGO aerogel, green lines for BiOBr powder).

maintained a high TOC level of 272.61 mg/L. The degradation of RhB under pure irradiation can be ignored (Figure 2c). The much higher photocatalytic activity over the BiOBr/RGO aerogel, as compared with that of BiOBr powder, can be attributed to the following factors. First, the BiOBr/RGO aerogel shows a higher adsorption capability toward RhB than the pure BiOBr powder due to its larger BET specific surface area and spongy nature. Usually, a photocatalyst with a large BET specific surface area is beneficial for its adsorption toward the pollutants, which is a prerequisite for high photocatalytic degradation.[29] As shown in Figure S5 (Supporting Information), 24% of RhB can be adsorbed over the BiOBr/RGO aerogel whereas only 4% over the pure BiOBr powder. Second, the BiOBr/RGO aerogel can absorb more visible light than pure BiOBr because it can float on the surface of the aqueous reaction system. Third, RGO in the aerogel can promote the charge transfer and help to separate the photogenerated charge carriers on BiOBr, which is beneficial for the photocatalysis.[39−42] It was found that the BiOBr/RGO aerogel can maintain a relatively high electrical conductivity to promote the charge transfer (33.2 S/m).

The BiOBr/RGO aerogel in monolithic shape can be easily recycled without loss of any solid photocatalysts after the aqueous photocatalytic reaction. As shown in Figure 2d, BiOBr can be facilely separated for recycling using a tweezer and after five cycles; no obvious decrease of the photocatalytic activity was observed over the BiOBr/RGO aerogel. On the contrary, although BiOBr is also stable during the photocatalytic reaction, the recycling process via filtration led to inevitable loss of partial photocatalyst (Figure 2e). After five cycles, only 68% of the original photocatalytic activity can be maintained (Figure 2f). Therefore, in addition to its superior photocatalytic performance, the BiOBr/RGO aerogel also shows good recyclability, which is especially important for practical application.

The one-pot method in the formation of BiOBr/RGO aerogel can also be applied to the preparations of other semiconductor photocatalysts embedded RGO composite aerogels. Well-shaped RGO composite aerogels containing metal oxides like Fe_2O_3, metal sulfides like CdS as well as other bismuth oxyhalides like BiOCl and BiOI can all be obtained via similar one-pot hydrothermal reactions (Figure 3a−h). For example, a CdS/RGO aerogel with a diameter of 25 mm and ca. 30 mm in height can be obtained from the reaction between GO and $Cd(NO_3)_2$ (inset of Figure 3a), whereas an Fe_2O_3/RGO aerogel ca. 18 mm in diameter and ca. 28 mm in height can be obtained from the reaction between GO and $Fe(NO_3)_3$ (inset of Figure 3c). The comparisons of the detailed properties of different semiconductor embedded RGO aerogels, including the semiconductor content in the composite, density, BET surface area and bulk electrical conductivity are shown in Table S1 (Supporting Information).

CONCLUSIONS

In summary, BiOBr/RGO aerogel was obtained via a facile one-pot method using lysine as a reducing agent and cross-linker. the BiOBr/RGO aerogel showed superior activity for the degradation of pollutants in aqueous system due to its improved adsorption toward pollutants owing to its large BET specific surface area and spongy nature, enhanced light absorption ascribed to its extremely lightweight as well as the promoted photogenerated charge separation by RGO. The aerogel also showed high stability and can be easily separated from the reaction systems for recycling. The facile one-pot method in the formation of BiOBr/RGO aerogels has been proved to be a generic method for the preparation of other semiconductor photocatalysts embedded RGO aerogels. The embedding of the semiconductor photocatalysts in the RGO aerogel may open a new avenue for the development high

DOI: 10.1021/sc5006473
ACS Sustainable Chem. Eng. 2015, 3, 277−282

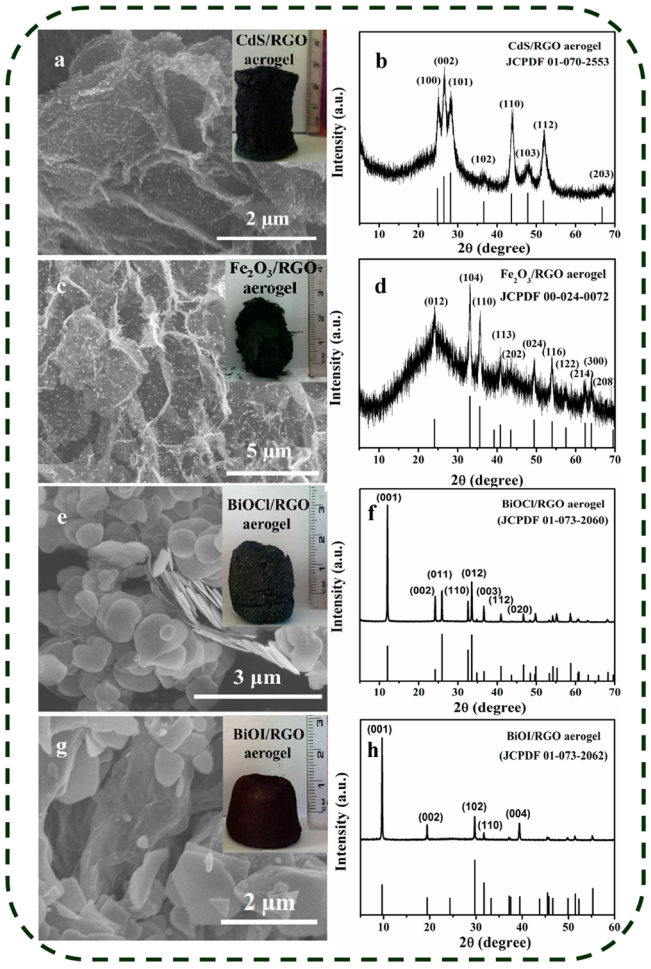

Figure 3. (a) SEM image (inset photograph) and (b) XRD pattern of CdS/RGO aerogel; (c) SEM image (inset photograph) and (d) XRD pattern of Fe_2O_3/RGO aerogel; (e) SEM image (inset photograph) and (f) XRD pattern of BiOCl/RGO aerogel; (g) SEM image (inset photograph) and (h) XRD pattern of BiOI/RGO aerogel.

efficiency photocatalysts that combine the advantages of enhanced activity with facile recycling for applications in aqueous photocatalytic reaction systems.

■ ASSOCIATED CONTENT

Ⓢ Supporting Information

Photographs of BiOBr/RGO hydrogels with different BiOBr concentrations, FTIR spectra and Raman spectra of GO and BiOBr/RGO aerogel, XPS spectra in C 1s region for BiOBr/RGO aerogel, nitrogen adsorption-desorption isotherms of as-synthesized BiOBr/RGO aerogel and BiOBr, temporal absorption spectral patterns of RhB during the photodegradation process over pure RGO aerogel, comparison of the temporal changes of RhB concentration as monitored by the UV−vis absorption spectra at 554 nm over BiOBr/RGO aerogel and BiOBr powder in the dark, and conductivity, BET surface area, semiconductor content and density of different semiconductor embedded RGO aerogels. This material is available free of charge via the Internet at http://pubs.acs.org.

■ AUTHOR INFORMATION

Corresponding Author

*Z. Li. E-mail: zhaohuili1969@yahoo.com. Tel (Fax): 86-591-83779260.

Notes

The authors declare no competing financial interest.

■ ACKNOWLEDGMENTS

The work was supported by NSFC (21273035), 973 Programs (2014CB239303) and Specialized Research Fund for the Doctoral Program of Higher Education (20123514110002). Z. Li thanks the Award Program for Minjiang Scholar Professorship for financial support.

■ REFERENCES

(1) Kistler, S. S. Coherent expanded aerogels and jellies. *Nature* **1931**, *127*, 741−742.
(2) Worsley, M. A.; Kucheyev, S. O.; Mason, H. E.; Merrill, M. D.; Mayer, B. P.; Lewicki, J.; Valdez, C. A.; Suss, M. E.; Stadermann, M.; Pauzauskie, P. J., Jr.; S, J. H.; Biener, J.; Baumann, T. F. Mechanically robust 3D graphene macroassembly with high surface area. *Chem. Commun.* **2012**, *48*, 8428−8430.
(3) Pham, H. D.; Pham, V. H.; Cuong, T. V.; Phan, T. D. N.; Chung, J. S.; Shin, E. W.; Kim, S. Synthesis of the chemically converted graphene xerogel with superior electrical conductivity. *Chem. Commun.* **2011**, *47*, 9672−9674.
(4) Li, C.; Shi, G. Q. Functional gels based on chemically modified graphenes. *Adv. Mater.* **2014**, *26*, 3992−4012.
(5) Chabot, V.; Higgins, D.; Yu, A. P.; Xiao, X. C.; Chen, Z. W.; Zhang, J. J. A review of graphene and graphene oxide sponge: Material synthesis and applications to energy and the environment. *Energy Environ. Sci.* **2014**, *7*, 1564−1596.
(6) Cong, H. P.; Chen, J. F.; Yu, S. H. Graphene-based macroscopic assemblies and architectures: An Emerging Material System. *Chem. Soc. Rev.* **2014**, *43*, 7295−7325.
(7) Wang, R. H.; Xu, C. H.; Sun, J.; Gao, L.; Yao, H. L. Solvothermal-induced 3D macroscopic SnO_2/nitrogen-doped graphene aerogels for high capacity and long-life lithium storage. *ACS Appl. Mater. Interfaces* **2014**, *6*, 3427−3436.
(8) Nardecchia, S.; Carriazo, D.; Ferrer, M. L.; Gutiérrez, M. C.; del Monte, F. Three Dimensional macroporous architectures and aerogels built of carbon nanotubes and/or graphene: Synthesis and applications. *Chem. Soc. Rev.* **2013**, *42*, 794−830.
(9) Bi, H. C.; Huang, X.; Wu, X.; Cao, X. H.; Tan, C. L.; Yin, Z. Y.; Lu, X. H.; Sun, L. T.; Zhang, H. Carbon microbelt aerogel prepared by waste paper: An efficient and recyclable sorbent for oils and organic solvents. *Small* **2014**, *10*, 3544−3550.
(10) Liu, W. J.; Wang, Y. K.; Li, Z. H. Tuning of surface wettability of RGO-based aerogels for various adsorbates in water using different amino acids. *Chem. Commun.* **2014**, *50*, 10311−10314.
(11) Li, Y. Q.; Samad, Y. A.; Polychronopoulou, K.; Alhassan, S. M.; Liao, K. Carbon aerogel from winter melon for highly efficient and recyclable oils and organic solvents absorption. *ACS Sustainable Chem. Eng.* **2014**, *2*, 1492−1497.
(12) Biener, J.; Stadermann, M.; Suss, M.; Worsley, M. A.; Biener, M. M.; Rose, K. A.; Baumann, T. F. Advanced carbon aerogels for energy applications. *Energy Environ. Sci.* **2011**, *4*, 656−667.
(13) Ye, S. B.; Feng, J. C. Self-assembled three-dimensional hierarchical graphene/polypyrrole nanotube hybrid aerogel and its application for supercapacitors. *ACS Appl. Mater. Interfaces* **2014**, *6*, 9671−9679.
(14) Tong, H.; Ouyang, S. X.; Bi, Y. P.; Umezawa, N.; Oshikiri, M.; Ye, J. H. Nano-photocatalytic materials: Possibilities and challenges. *Adv. Mater.* **2012**, *24*, 229−251.
(15) Chen, C. C.; Ma, W. H.; Zhao, J. C. Semiconductor-mediated photodegradation of pollutants under visible-light irradiation. *Chem. Soc. Rev.* **2010**, *39*, 4206−4219.
(16) Huang, X.; Tan, C.; Yin, Z.; Zhang, H. 25th anniversary article: Hybrid nanostructures based on two-dimensional nanomaterials. *Adv. Mater.* **2014**, *26*, 2185−2204.
(17) Liu, J. C.; Bai, H. W.; Wang, Y. J.; Liu, Z. Y.; Zhang, X. W.; Sun, D. D. Self-assembling TiO_2 nanorods on large graphene oxide sheets at

DOI: 10.1021/sc5006473
ACS Sustainable Chem. Eng. 2015, 3, 277−282

a two-phase interface and their anti-recombination in photocatalytic applications. *Adv. Funct. Mater.* **2010**, *20*, 4175−4181.
(18) Tu, W. G.; Zhou, Y.; Zou, Z. G. Versatile graphene-promoting photocatalytic performance of semiconductors: Basic principles, synthesis, solar energy conversion, and environmental applications. *Adv. Funct. Mater.* **2013**, *23*, 4996−5008.
(19) Xiang, Q. J.; Yu, J. G.; Jaroniec, M. Synergetic effect of MoS_2 and graphene as cocatalysts for enhanced photocatalytic H_2 production activity of TiO_2 nanoparticles. *J. Am. Chem. Soc.* **2012**, *134*, 6575−6578.
(20) An, X. Q.; Yu, J. C. Graphene-based photocatalytic composites. *RSC Adv.* **2011**, *1*, 1426−1434.
(21) Xiang, Q. J.; Yu, J. G.; Jaroniec, M. Graphene-based semiconductor photocatalysts. *Chem. Soc. Rev.* **2012**, *41*, 782−796.
(22) Meyer, T.; Priebe, J. B.; Silva, R. O. D.; Peppel, T.; Junge, H.; Beller, M.; Brückner, A.; Wohlrab, S. Advanced charge utilization from $NaTaO_3$ photocatalysts by multilayer reduced graphene oxide. *Chem. Mater.* **2014**, *26*, 4705−4711.
(23) Yang, M. Q.; Zhang, N.; Pagliaro, M.; Xu, Y. J. Artificial photosynthesis over graphene-semiconductor composites. Are we getting better? *Chem. Soc. Rev.* **2014**, *43*, 8240−8254.
(24) Qiu, B. C.; Xing, M. Y.; Zhang, J. L. Mesoporous TiO_2 nanocrystals grown in situ on graphene aerogels for high photocatalysis and lithium-ion batteries. *J. Am. Chem. Soc.* **2014**, *136*, 5852−5855.
(25) Zhang, Z. Y.; Xiao, F.; Guo, Y. L.; Wang, S.; Liu, Y. Q. One-pot self-assembled three-dimensional TiO_2-graphene hydrogel with improved adsorption capacities and photocatalytic and electrochemical activities. *ACS Appl. Mater. Interfaces* **2013**, *5*, 2227−2233.
(26) Gao, M. M.; Peh, C. K. N.; Ong, W. L.; Ho, G. W. Green chemistry synthesis of a nanocomposite graphene hydrogel with three-dimensional nano-mesopores for photocatalytic H_2 production. *RSC Adv.* **2013**, *3*, 13169−13177.
(27) Han, W. J.; Ren, L.; Gong, L. J.; Qi, X.; Liu, Y. D.; Yang, L. W.; Wei, X. L.; Zhong, J. X. Self-assembled three-dimensional graphene-based aerogel with embedded multifarious functional nanoparticles and its excellent photoelectrochemical activities. *ACS Sustainable Chem. Eng.* **2014**, *2*, 741−748.
(28) Ai, Z. H.; Ho, W. K.; Lee, S. C. Efficient visible light photocatalytic removal of NO with BiOBr-graphene nanocomposites. *J. Phys. Chem. C* **2011**, *115*, 25330−25337.
(29) Tu, X. M.; Luo, S. L.; Chen, G. X.; Li, J. H. One-pot synthesis, characterization, and enhanced photocatalytic activity of a BiOBr-graphene composite. *Chem.—Eur. J.* **2012**, *18*, 14359−14366.
(30) Song, S. Y.; Gao, W.; Wang, X.; Li, X. Y.; Liu, D. P.; Xing, Y.; Zhang, H. J. Microwave-assisted synthesis of BiOBr/graphene nanocomposites and their enhanced photocatalytic activity. *Dalton Trans.* **2012**, *41*, 10472−10476.
(31) Cheng, H. F.; Huang, B. B.; Wang, P.; Wang, Z. Y.; Lou, Z. Z.; Wang, J. P.; Qin, X. Y.; Zhang, X. Y.; Dai, Y. In situ ion exchange synthesis of the novel Ag/AgBr/BiOBr hybrid with highly efficient decontamination of pollutants. *Chem. Commun.* **2011**, *47*, 7054−7056.
(32) Lerf, A.; He, H. Y.; Forster, M. Structure of graphite oxide revisited. *J. Phys. Chem. B* **1998**, *102*, 4477−4482.
(33) Chua, C. K.; Pumera, M. Selective removal of hydroxyl groups from graphene oxide. *Chem.—Eur. J.* **2013**, *19*, 2005−2011.
(34) Iwase, A.; Ng, Y. H.; Ishiguro, Y.; Kudo, A.; Amal, R. Reduced graphene oxide as a solid-state electron mediator in Z-scheme photocatalytic water splitting under visible light. *J. Am. Chem. Soc.* **2011**, *133*, 11054−11057.
(35) Luzan, S. M.; Talyzin, A. V. Hydration of graphite oxide in electrolyte and non-electrolyte solutions. *J. Phys. Chem. C* **2011**, *115*, 24611−24614.
(36) Chen, S.; Zhu, J. W.; Wu, X. D.; Han, Q. F.; Wang, X. Graphene oxide-MnO_2 nanocomposites for supercapacitors. *ACS Nano* **2010**, *4*, 2822−2830.
(37) Zhang, X. T.; Sui, Z. Y.; Xu, B.; Yue, S. F.; Luo, Y. J.; Zhan, W. C.; Liu, B. Mechanically strong and highly conductive graphene aerogel and its use as electrodes for electrochemical power sources. *J. Mater. Chem.* **2011**, *21*, 6494−6497.
(38) Chen, C. C.; Ma, W. H.; Zhao, J. C. Photosensitized degradation of dyes in polyoxometalate solutions versus TiO_2 dispersions under visible-light irradiation: Mechanistic implications. *Chem.—Eur. J.* **2004**, *10*, 1956−1965.
(39) Krishnamurthy, S.; Kamat, P. V. Galvanic exchange on reduced graphene oxide: Designing a multifunctional two-dimensional catalyst assembly. *J. Phys. Chem. C* **2013**, *117*, 571−577.
(40) Huang, C. C.; Li, C.; Shi, G. Q. Graphene based catalysts. *Energy Environ. Sci.* **2012**, *5*, 8848−8868.
(41) Lee, M.; Yang, S.; Kim, K. J.; Kim, S.; Lee, H. Comparison of the catalytic oxidation reaction on graphene oxide and reduced graphene oxide. *J. Phys. Chem. C* **2014**, *118*, 1142−1147.
(42) Etacheri, V.; Yourey, J. E.; Bartlett, B. M. Chemically bonded TiO_2-bronze nanosheet/reduced graphene oxide hybrid for high-power lithium ion batteries. *ACS Nano* **2014**, *8*, 1491−1499.

DOI: 10.1021/sc5006473
ACS Sustainable Chem. Eng. 2015, 3, 277−282